Original Article

Overcoming drug resistance in Hepatocellular Carcinoma: preparation and mechanistic insights into a novel chalcone derivative

Yuanyuan Dai[1,2,3,4], Wenting Zhou[3,4], Jiazi Luo[3,4], Shixian Yang[1], Shumin Liang[5], Xibin Dou[3,4], and Yanqiang Huang[3,4,6,7]

[1]Center for Medical Laboratory Science, Affiliated Hospital of Youjiang Medical University for Nationalities, Guangxi, 533000, China.

[2]Baise Key Laboratory for Research and Development on Clinical Molecular Diagnosis for High-Incidence Diseases, Guangxi, 533000, China.

[3]Guangxi Zhuang Autonomous Region Engineering Research Center of Clinical Prevention, Control Technology and Leading Drug for Microorganisms with Drug Resistance in Border Ethnic Areas, Baise 533000, China.

[4]Guangxi Technology Innovation Cooperation Base of Prevention and Control Pathogenic Microbes with Drug Resistance, Youjiang Medical University for Nationalities, Baise 533000, China.

[5]School of Languages and Culture, Youjiang Medical University for Nationalities, Baise 533000, China.

[6]Key Laboratory of the Prevention and Control of Drug-resistant Microbial Infection in Guangxi, Baise 533000, China.

[7]Guangxi Key Laboratory of Basic Research in Prevention and Treatment for Helicobacter pylori, Baise 533000, China.

Correspondence to: Prof. Xibin Dou, Guangxi Technology Innovation Cooperatio n Base of Prevention and Control Pathogenic Microbes with Drug Resistance, Yo

DOI: 10.20517/scierxiv202505.0135.v1 https://www.scierxiv.com/

ujiang Medical University for Nationalities, Baise 533000, China. E-mail: doctordxb@163.com

ORCID: Prof. Xibin Dou (0009-0009-6759-4142).

Received: 15 March 2025 | Approved: 08 May 2025 | Online: 08 May 2025

Abstract

Aim: Chalcone derivatives exhibit anti-hepatoma potential but are limited by low efficacy and poor solubility. The study designed a novel chalcone derivative (GD-Chalcone) to enhance solubility, anti-tumor activity, and its ability to overcome drug resistance in Hepatocellular carcinoma (HCC).

Methods: GD-Chalcone was synthesized via substitution and reduction reactions, and characterized by MS and NMR. In-vitro anti-hepatoma activity was assessed using Cell Counting Kit-8 (CCK-8) and Transwell migration/invasion assays. Drug resistance-related PI3K/AKT pathways were analyzed via RT-qPCR. In vivo efficacy and gut microbiota modulation were evaluated in chemically induced HCC mice.

Results: GD-Chalcone showed two-fold higher solubility (0.625 μM/mL). It also showed a significant increase in antitumor activity, with half-maximal inhibitory concentrations (IC_{50}) against HCC cells SMMC-7721 and HuH-7 being 82.5 ± 2.15 μM and 34.30 ± 1.53 μM, respectively. Notably, GD-Chalcone showed potent efficacy against drug-resistant HCC cells (IC_{50}: 28.7 ± 1.27 μM), while its effect on gastric cancer cells was limited. It suppressed HCC migration/invasion and downregulated Bcl-2. In vivo, GD-Chalcone outperformed sorafenib (Sor) in tumor suppression and microbiota regulation.

Conclusion: GD-Chalcone may overcomes drug resistance via PI3K/AKT inhibition

and microbiota modulation, offering a novel strategy for resistant HCC therapy.

Keywords: Chalcone derivatives; hepatocellular carcinoma; drug resistance; PI3K/AKT pathway; gut microbiota

INTRODUCTION

Hepatocellular carcinoma (HCC), with a continuously rising incidence, is a global health concern. The mortality rate of HCC among Chinese individuals ranks second among malignant tumors, following lung cancer[1,2]. Due to its insidious metastasis and high recurrence rate, many patients are diagnosed only at the mid-to-late stages. This results in poor prognosis and limits the effectiveness of current treatment options, rendering intervention challenging[3,4]. With the increasing demand for HCC treatment, existing chemotherapy and targeted therapies face issues such as drug resistance, lack of specificity, and insufficient efficacy[5,6]. Therefore, there is an urgent need to develop novel therapeutic strategies, particularly those targeting drug resistance mechanisms to improve treatment outcomes.

Drug resistance in HCC is a major obstacle in clinical therapy,often leading to treatment failure and disease progression. One of the primary mechanisms contributing to drug resistance is the activation of the PI3K/AKT signaling pathway, which promotes cell survival, proliferation, and resistance to apoptosis[7]. Additionally, overexpression of anti-apoptotic proteins such as Bcl-2, increased drug efflux mediated by ATP-binding cassette (ABC) transporters, and tumor microenvironment adaptations further contribute to resistance against conventional therapies[8]. Consequently, overcoming drug resisitance is a critical challenge in the development of effective HCC treatment.

Screening and modifying active ingredients from natural sources has become an efficient method for developing novel drugs[9,10]. In recent years, flavonoids derived from natural products have gained attention due to their diverse pharmacological effects,

including anti-oxidation, blood pressure regulation, and antitumor activity[11,12]. Among these compounds, isoprenylated flavonoids have emerged as promising agents for cancer treatment due to their significant antitumor activity at various stages of tumor development[13].

Isobavachalcone (IBC), an isoprenylated flavonoid compound widely used in traditional Chinese medicine (TCM), has attracted attention due to its low tendency to induce drug resistance and its diverse pharmacological effects, including anti-inflammatory, antibacterial, antioxidant, and antitumor properties[14]. Although various pharmacological activities of IBC have been confirmed, its specific mechanisms of action remain incompletely understood, and its inhibitory effects on different tumors types vary significantly. This highlights the need for further research to clarify IBC's antitumor potential and enhance its therapeutic efficacy against HCC.

This study introduces the synthesis and characterization of a novel chalcone derivative, GD-Chalcone, designed to enhance solubility, anti-tumor activity, and its ability to overcome drug resistance in HCC. Preliminary screening revealed that while IBC exhibited cytotoxic effects against HCC cells, its efficacy required enhancement. Structural modifications led to the development of GD-Chalcone, which demonstrated improved antitumor activity, higher solubility, and superior efficacy against drug-resistant HCC cells. By investigating the potential of GD-Chalcone to inhibit HCC progression and modulate drug resistance mechanisms, this research provides a scientific foundation for developing more effective HCC therapies.

METHODS

Cell culture

In the present study, the HCC cell lines SMMC-7721 and HuH-7 were purchased from the Stem Cell Bank, Chinese Academy of Sciences. The HepG2.2.15 sorafenib-resistant HCC cell line was obtained from BLUEFBIO™. SMMC-7721 and HuH-7 cells were

cultured in RPMI 1640 complete medium containing 10% fetal bovine serum (FBS) and 1% penicillin-streptomycin (KeyGEN BioTECH, Shanghai). HepG2.2.15 cells were maintained in DMEM (Invitrogen 12430) supplemented with 10% ES-grade FBS (Biochrom S4115), 90 mM GlutaMAX (Invitrogen 35050), 6 mL NEAA (Invitrogen 11140), 6 mL LIF (Millipore ESG1107), 60 μL β-Mercaptoethanol (Invitrogen 21985, 1000 U/mL). All cells were maintained in a humidified incubator at 37 ℃ with 5% CO_2.

Preparation of GD-Chalcone

Under stirring at 0 °C, IBC (65 mg), potassium carbonate (155-165 mg; K_2CO_3), and bromoglucoside (246 mg) were sequentially added to acetonitrile (20 mL; ACN). The resulting mixture reacted at room temperature for 15 h. The reaction completion was determined using a thin layer chromatography (TLC). After the reaction, the mixture was quenched with a saturated ammonium chloride (NH_4Cl) solution. The organic phase was extracted with ethyl acetate (EA), washed with saturated brine, dried over anhydrous sodium sulfate (Na_2SO_4), filtered, and concentrated.

4-acetylglucosyl-2',4'-dihydroxy-3'-isopentenyl chalcone (44 mg) was purified using a silica (Si) gel, dissolved in anhydrous methanol (10 mL; MeOH), and stirred at 0 °C. The resulting solution was treated with sodium methoxide (26-36 mg), and the reaction was carried out in an ice bath for 4-5 h. Thereafter, it was treated with acetic acid (1 mL; AA), filtrated and concentrated. The resulting product was purified using HPLC, yielding a new chalcone derivative, a bright yellow solid powder.

Detection of half-maximal inhibitory concentrations (IC_{50})

Hepatocellular carcinoma cells (SMMC-7721, HuH-7, and HepG2) and gastric cancer (GC) cells (MGC803) were cultured in a 96-well plate (each at a density of 2×10^4 per well). After 24 h of treatment with different concentrations of the drug, 10 μL of the CCK8 solution (Beyotime Biotechnology, Shanghai) was added to each well, thoroughly mixed, and incubated for 4 h at 37 °C in the dark. After incubation, the

DOI: 10.20517/scierxiv202505.0135.v1 https://www.scierxiv.com/

absorbance at 450 nm was measured using a microplate reader. Cell viability was calculated, and the IC_{50} value of the drug was determined.Cell viability was calculated using the formula: [(As − Ab)] / [(Ac − Ab)] × 100%, where As represents the absorbance of the drug-treated wells, Ac represents the absorbance of the untreated wells, and Ab represents the absorbance of the wells containing neither cells nor the drug. The experiment was performed in triplicate.

Transwell assay

SMMC-7721 cells were serum-starved in serum-free medium for 12-24 h, resuspended in a serum-free RPMI 1640 medium, and counted. Thereafter, the cell density was adjusted to 5×10^5 cells/mL. Transwell inserts were placed into a 24-well plate using tweezers. Each well of the lower compartment was filled with the RPMI 1640 complete medium supplemented with 10% FBS (600 μL), and each insert (upper compartment) was loaded with the cell suspension (200 μL). After drug treatment, the plate was incubated at 37°C in a 5% CO_2 incubator for 12-48 h. Following incubation, the cells were fixed and stained, and the Gram-positive cells that had been dyed purple were observed and counted using an inverted microscope. Photos were taken, and the results were statistically analyzed.

Scratch assay

SMMC-7721 cells in the logarithmic phase were seeded in a six-well plate (5×10^5 cells per well) and incubated for 24 h. Straight lines were gently scratched in the bottom of the culture dish using a pipette tip. The cells were washed with phosphate-buffered saline (PBS) to remove cellular debris dislodged during scratching. The cells were then treated with serum-free medium containing drugs at different concentrations, and incubated for 0, 6, 12, and 24 h. Cell migration was recorded using an inverted microscope, and the migration areas at different time points were calculated.

Clonogenic assay

DOI: 10.20517/scierxiv202505.0135.v1

SMMC-7721 cells (700 cells per well) were seeded in a six-well plate. After 24 h of incubation, the cells were treated with GD-Chalcone at different concentrations. The positive control drugs IBC and cisplatin (CDDP) were used for comparison. The samples were incubated (100% humidity) at 37 °C in an atmosphere of 5% CO_2 for 14 d. During this period, the drug-containing medium was replaced every 2-3 d, and the cell conditions were monitored. Thereafter, the samples were fixed with 4% formaldehyde solution (Biosharp, Anhui), stained with 0.1% crystal violet solution (Macklin, Shanghai), washed using PBS, and dried. The colonies, developed from cells, were counted using the ImageJ software based on the stained cells.

Flow cytometry (FCM)-based apoptosis detection

After 24 h of drug treatment, the culture medium of Hep-G2 and HuH-7 cells was pipetted into centrifuge tubes for later use. Adherent cells were detached by adding trypsin (TRY), and the digestion was terminated by adding the collected culture medium. The cells were then centrifuged at 1,000 × g for 5 min, and the supernatant was discarded. Thereafter, the cells were washed with PBS, resuspended and counted, with their concentration being adjusted to 1 × 10^5 cells/mL. They were then recentrifuged at 1,000 × g for 5 min, and the supernatant was discarded. Subsequently, the cells were gently resuspended in 195 μL of Annexin V Fluorescein Isothiocyanate (Annexin V-FITC) binding buffer (Beyotime Biotechnology, Shanghai), and treated with Annexin V-FITC (5 μL) and propidium iodide (PI) staining solution (10 μL; Beyotime Biotechnology, Shanghai). They were incubated at room temperature in the dark for 20 min and then immediately analyzed using FCM.

Cell cycle analysis using FCM

Hep-G2 and HuH-7 cells treated with drugs for 24 h were digested using TRY, collected, and centrifuged at 1,000 × g for 5 min, and the supernatant was discarded. The cells were resuspended in the pre-chilled PBS (1 mL) and recentrifuged at 1,000 × g for 5 min, and the supernatant was discarded. The cell pellets were then fixed

DOI: 10.20517/scierxiv202505.0135.v1

overnight in the pre-chilled 70% ethanol (EtOH). After fixation, the cells were centrifuged at 1,000 × g for 5 min, with the supernatant being discarded, and treated with the previously prepared PI staining solution (0.5 mL; Beyotime Biotechnology, Shanghai). Thereafter, the cells were gently resuspended, incubated at 37 °C in the dark for 30 min, and subsequently analyzed using FCM.

Establishment of mice models with hepatoma

SPF C57BL/6J mice aged 6 weeks were treated with diethylnitrosamine (DEN; 10 mg/kg; MedChemExpress, Shanghai) through oral gavage once a week, consecutively for 18 weeks. The mice had access to drinking water containing 0.025% DEN for 6 d each week, and normal drinking water on the 7th d. From the 18th-23rd weeks, mice were treated daily through oral gavage with GD-Chalcone (either 20 or 40 mg/kg) or sorafenib (Sor; 20 mg/kg). During the treatment period, the body weights of the mice were recorded, and fecal samples were collected. Blood was collected from the retro-orbital sinus and liver tissue was harvested within 72 h after the final treatment.

Hematoxylin and eosin (H&E) Staining

Paraffin sections (4-5 μm in thickness) were dewaxed with xylene (10 min; twice) and EtOH at different concentrations (100%, 95%, and 70%, each for 5 min), and then rinsed in distilled water. They were stained with hematoxylin solution for 3-5 min, differentiated in a weak acid solution (1% hydrochloric acid in EtOH) for 10-30 s to remove excess dye, and blued by rinsing in running water for 5-10 min. The sections were then stained with eosin solution for 1-2 min, dehydrated through 70%, 95%, and 100% EtOH (each for 5 min), cleared in xylene (5 min; twice), and mounted with a neutral mounting medium. Finally, tissue morphology and cellular structure were examined using a light microscope (LM).

Immunohistochemistry (IHC) detection

The paraffin sections were first dewaxed via sequential immersion in environmentally

DOI: 10.20517/scierxiv202505.0135.v1

friendly deparaffinization agents (I, II, and III, each for 10 min), and treated with anhydrous EtOH (I, II, and III, each for 5 min). Thereafter, the sections were washed using distilled water, and after antigen retrieval, they were washed thrice using PBS (pH 7.4), each for 5 min. The sections were incubated in 3% hydrogen peroxide (H_2O_2) solution in the dark for 25 min, and washed using PBS. Subsequently, 3% bovine serum albumin (BSA) or normal rabbit serum was added to the slides within a rim drawn with a pencil for creating a hydrophobic barrier, and incubated at room temperature for 30 min. After blocking, the slides were treated with the primary antibody (diluted to 1:100) and incubated overnight at 4°C. On the following day, the slides were washed thrice using PBS, treated with the corresponding species-specific secondary antibody (HRP [horseradish peroxidase]-labeled), and incubated at room temperature for 50 min. Thereafter, the sections were washed using PBS, treated with freshly prepared 3,3'-diaminobenzidine (DAB) substrate for chromogenic development, and observed under a microscope. Positive signals presented as brownish-yellow. The chromogenic reaction was terminated by rinsing in tap water. The cell nuclei were counterstained with hematoxylin for 3 min, differentiated briefly, and blued. The slides were dehydrated sequentially in 75% EtOH, 85% EtOH, absolute EtOH, and n-butanol ($C_4H_{10}O$). They were then cleared in xylene, and mounted with a coverslip. The experimental results were evaluated using a LM, where the cell nuclei appeared blue and the positive signals were brownish-yellow.

Cytotoxicity assay

NRK-52E and fibroblast cells were seeded into a 96-well plate, cultured to the logarithmic phase, treated with GD-Chalcone at different concentrations, and cultured for 24 h. The cell viability was determined using the CCK8 assay. With the untreated group used as a control, the drug-induced inhibition rate of cell proliferation was calculated.

Hemolysis assay

DOI: 10.20517/scierxiv202505.0135.v1

The blood samples were centrifuged at 3,000 rpm for 5 min to separate the red blood cells (RBCs) and plasma. The collected RBCs were washed with PBS for several times and diluted to 10% of PBS solution for later use. Control groups included: 10% RBC suspension (200 μL) mixed with PBS (1 mL), and 10% RBC suspension (200 μL) mixed with ddH_2O (1 mL). In the experimental groups, GD-Chalcone dissolved in 1 mL PBS at different concentrations was mixed with 10% RBC suspension (200 μL). The mixtures were incubated at 37 °C for 24 h, and centrifuged at 3,000 rpm for 10 min. The supernatant was measured at 541 nm to assess hemolysis. The percentage of hemolysis was calculated using the formula: (As − Aso − Anc) / (Apc − Anc) × 100%, where As, Aso, Anc, and Apc represent the absorbance at 541 nm for the supernatants from RBC-containing samples, RBC-free samples, the negative control, and the positive control, respectively.

Intestinal microbiota assay

Genomic DNA was first extracted from fecal samples, and its integrity was verified using agarose gel electrophoresis. Subsequently, PCR amplification was performed using specific primers, and the PCR products were detected and purified via electrophoresis. During the library construction phase, adapters were ligated to the DNA fragments, and self-ligated adapter fragments were removed using magnetic beads. PCR amplification was used to enrich the library, and single-stranded DNA (ssDNA) fragments were sequenced using a sequencing platform. Thereafter, sequence information was obtained through fluorescence signal readout and chemical cleavage methods. This process provided foundational data for analyzing the composition and diversity of the intestinal microbiota.

Network pharmacology analysis of GD-Chalcone

The structure of the GD-Chalcone compound was drawn on the SwissTarget Prediction platform (http://www.swisstargetprediction.ch/) to obtain its simplified molecular input line entry system (SMILES), and the potential drug targets were predicted. Thereafter,

the disease-related targets were retrieved from the GeneCards database (www.genecards.org/) using the keyword “liver cancer (LC)”.

The intersection between the predicted targets of GD-Chalcone and those associated with liver cancer was identified to determine the potential common targets for the treatment of LC with GD-Chalcone. Protein-protein interaction (PPI) data for the targets were obtained from the Search Tool for the Retrieval of Interacting Genes/Proteins (STRING) database (https://cn.string-db.org/), and a protein interaction network was constructed using data from the OmicStudio platform (https://www.omicstudio.cn/). The Gene Ontology (GO) and Kyoto Encyclopedia of Genes and Genomes (KEGG) analyses of the identified genes were performed using the Database for Annotation, Visualization, and Integrated Discovery (DAVID). GO and KEGG bubble plots were generated using the R package “ggplot2”.

Molecular docking

The specific binding modes of GD-Chalcone with the selected potential targets were analyzed via molecular docking using the AutoDock Vina software, where the selected template-based protein structure modeling was completed. The resulting protein models were docked with GD-Chalcone. The docking results were then visualized using Python Molecular Graphics (PyMOL) and LigPlot to illustrate the active site pockets. The binding modes were scored based on kinematic principles, and the highest-scoring one was selected to represent the binding affinity between GD-Chalcone and the target protein.

Real-time PCR assay

The number of HCC SMMC-7721 cells was adjusted to 1×10^6 and cultured for 12 h. Subsequently, IBC was added at a concentration equivalent to 10 times its IC_{50}, followed by an additional 12-hour incubation. After incubation, the cells were harvested via centrifugation, and total RNA was extracted using the SevenFast Total RNA

DOI: 10.20517/scierxiv202505.0135.v1

Extraction Kit for Cells (SEVEN, China) following cell lysis. The extracted RNA was then reverse-transcribed into complementary DNA using a reverse transcription kit (MONPURE, China). Real-time PCR (RT-qPCR) was conducted using the LightCycler system in accordance with the manufacturer's instructions (MONPURE, China). The cycling conditions were as follows: pre-denaturation at 95 °C for 30 s, denaturation at 95 °C for 10 s, and annealing/extension at 60 °C for 30 s (40 cycles). The 16S ribosomal RNA amplicon served as an internal control, and relative quantification was employed to normalize data and assess expression level changes. The primer sequences are listed in Table 1. The relative mRNA expression levels were calculated using the $2^{-\Delta\Delta Cq}$ method.

Table 1. Primers used for reverse transcription-quantitative polymerase chain reaction

Gene	Primer	Sequence
Bax	Forward	5’-GCGAATTGGAGATGAACT-3’
	Reverse	5’-GTGAGCGAGGCGGTGAGGAC-3’
Bcl-2	Forward	5’-GGTTGCCTTATGTATTTGTTTG-3’
	Reverse	5’-CCTCCGCAATGCTGAAAG-3’
GAPDH	Forward	5’-AATCTCATCACCATATTCCA-3’
	Reverse	5’-CCTGCTTCACCACCTTGTTG-3’

Statistical analysis

Statistical analysis was performed using the SPSS software, Version 26.0. Continuous data were expressed as mean ± SD. Differences between groups were analyzed using the *t*-test, while multiple groups were compared using the single factor variance analysis. $P < 0.05$ was considered statistically significant.

RESULTS

GD-Chalcone preparation

The modification was carried out by introducing glucose at the hydroxyl group (-OH) via substitution and reduction reactions. The resulting product was a chalcone derivative (GD-Chalcone) with a molecular weight of 486.517 (Figures 1A and B). It emerged as a pale yellow powder and exhibited higher solubility than did the original compound (Figures 1C and D). LC-MS analyses revealed that at a wavelength of 254 nm, the purity of GD-Chalcone was 100%. In the positive ion mode, the molecular weight of 486.9 corresponds to M + H, 508.8 corresponds to M + Na, and the results matched the target structure (Figures 1E-G). Additionally, NMR and FTIR spectroscopy were employed for further verification, confirming the successful synthesis (Figures S1-3).

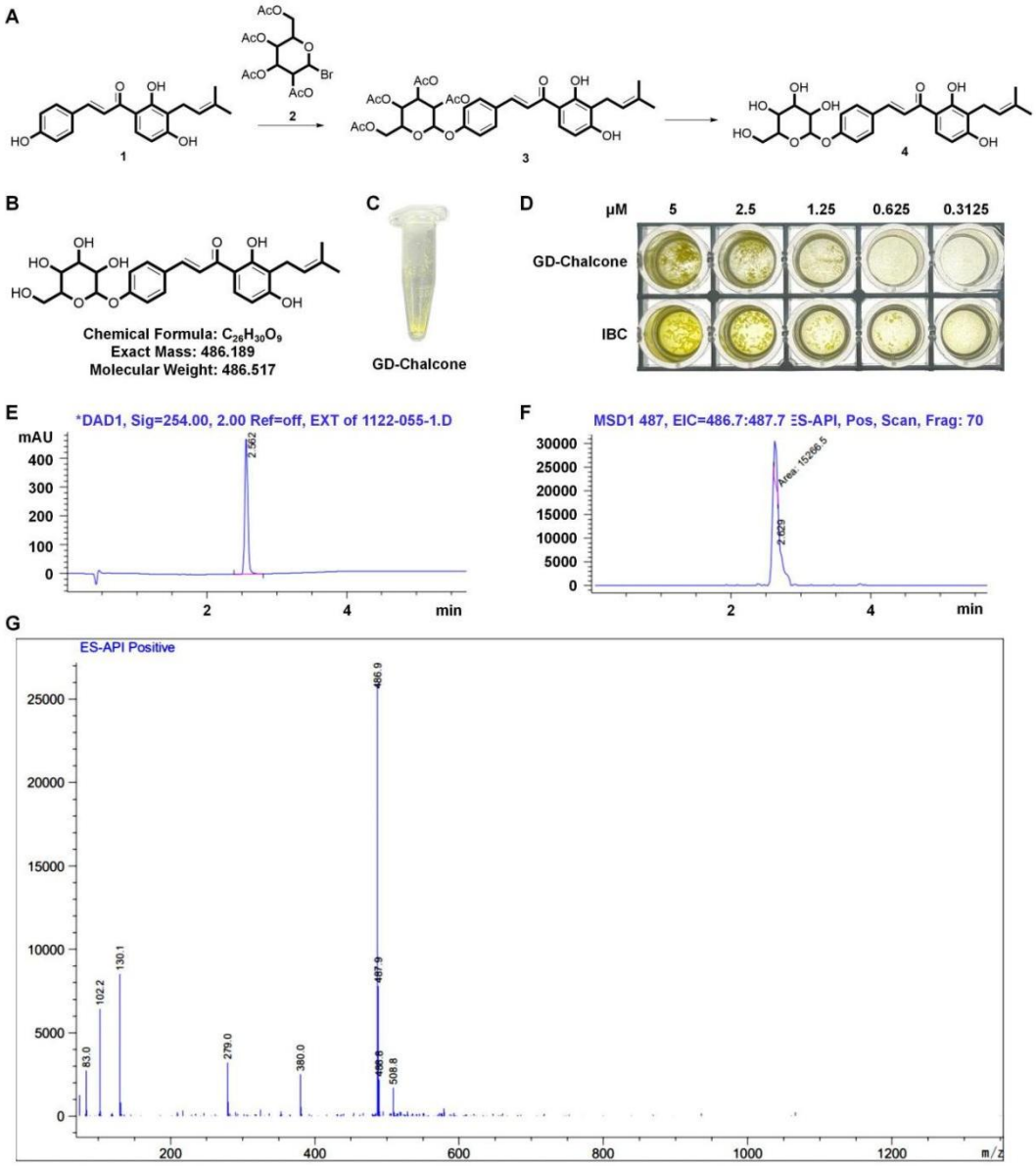

DOI: 10.20517/scierxiv202505.0135.v1

Figure 1. Preparation of the chalcone derivative. A: Synthetic procedures for GD-Chalcone; B. Molecular structure of GD-Chalcone; C. GD-Chalcone presenting as a pale yellow powder; D. Comparison of solubility between GD-Chalcone and IBC; E. HPLC-diode array detection (DAD) analyses of GD-Chalcone; F. Gas chromatography (GC)-MS analyses of GD-Chalcone; G. LC-MS analyses of GD-Chalcone.

Activity of GD-Chalcone in inhibiting the proliferation and migration of HCC cells

The inhibitory activity of GD-Chalcone, with improved solubility, against tumor cell proliferation was compared before and after modification using the CCK8 assay. The results showed that GD-Chalcone had an IC_{50} value of 82.5 ± 2.15 μM for SMMC-7721 cells and 86.93 ± 1.97 μM for HepG2.2.15 cells, which were 3-4 times lower than those of the pre-modified form. Its activity against HuH-7 cells was also significantly improved, demonstrating an efficacy comparable to that of CDDP (Table 2). Notably, GD-Chalcone remained effective even in sorafenib-resistant cells, highlighting its potential in overcoming drug resistance. These findings suggest that GD-Chalcone may serve as a promising anti-tumor agent with enhanced potency. This conclusion was further supported by Transwell, scratch, and clonogenic assays, which confirmed that GD-Chalcone more effectively inhibited the proliferation and migration of HCC cells compared to its pre-modified form (Figures 2A-F).

Table 2. IC_{50} values of CDDP, IBC and GD-Chalcone on tumor cells (μM)

Compound	SMMC-7721	HuH-7	HepG2.2.15	MGC803
CDDP	16.85 ± 1.45	34.82 ± 1.54	18.47 ± 1.68	19.72 ± 1.61
IBC	277.92 ± 1.36	49.91 ± 1.69	316.27 ± 2.09	24.83 ± 1.22
GD-Chalcone	82.5 ± 2.15	34.30 ± 1.53	86.93 ± 1.97	101.62 ± 1.96

Induction of apoptosis and synthesis (S) phase arrest in HCC cells by GD-Chalcone

DOI: 10.20517/scierxiv202505.0135.v1

To further investigate the inhibitory effects of GD-Chalcone on HCC cell growth, we analyzed apoptosis and cell cycle distribution using FCM. Compared with the control groups, the number of early and late apoptotic cells increased with increasing concentrations of GD-Chalcone, indicating that GD-Chalcone promoted HCC cell apoptosis in a dose-dependent manner. Moreover, the pro-apoptotic activity was higher than that of the pre-modified form (Figures 3A and C). The cell cycle analysis also showed that, compared with the control groups, HCC cells treated with GD-Chalcone exhibited a significant increase in the S phase (the DNA replication stage) and a decrease in the Gap 2 (G2)/mitosis (M) phase. This indicated that GD-Chalcone arrests HCC cells in the S phase, affects DNA replication and inhibits cell proliferation[15] (Figures 3B and D). These results suggested that GD-Chalcone may inhibit the malignant growth of human HCC cells by inducing apoptosis and arresting the cell cycle in the S phase.

DOI: 10.20517/scierxiv202505.0135.v1

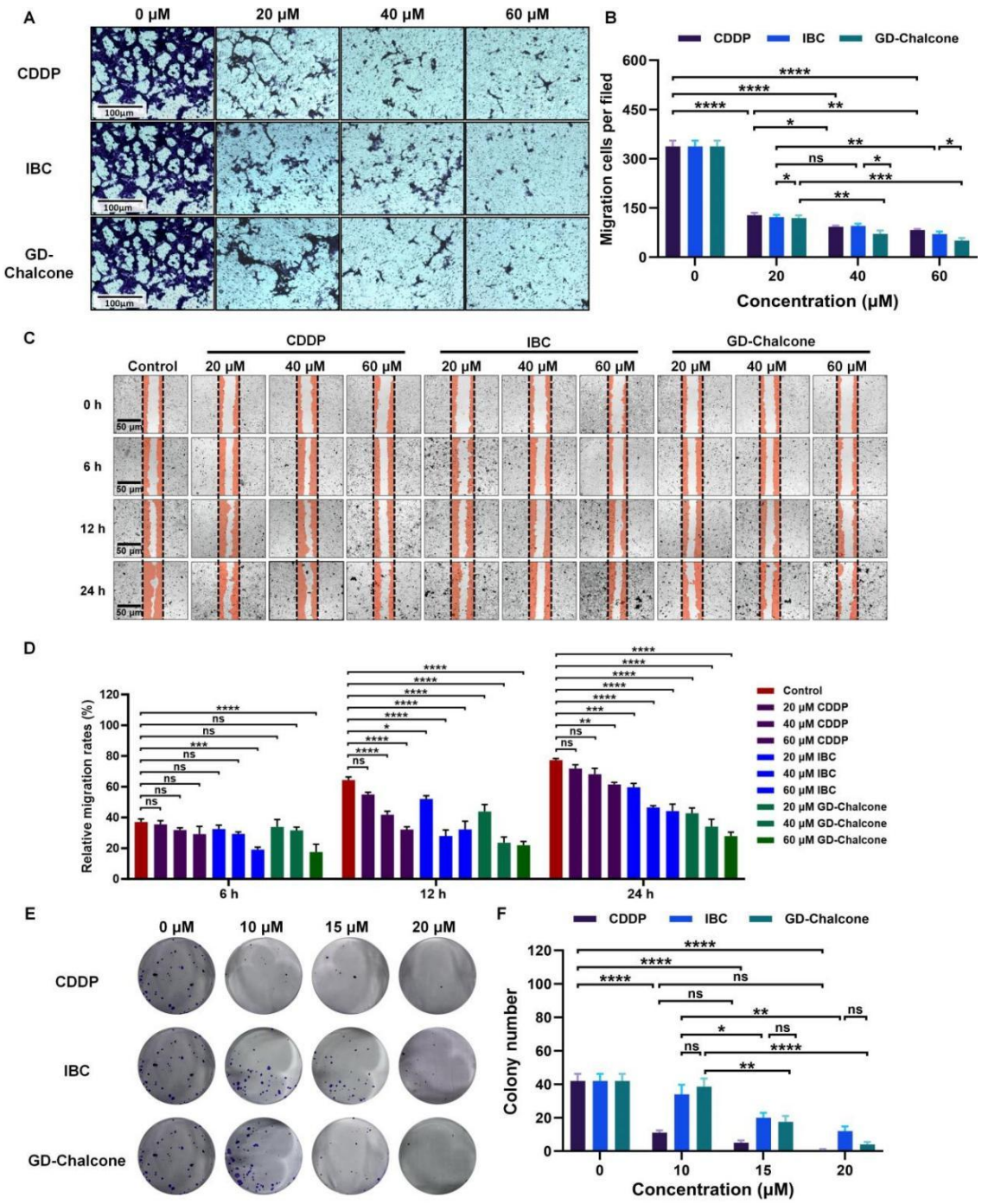

Figure 2. Effects of GD-Chalcone on the proliferation of HCC cells. A: Inhibition of HCC cell migration *in vitro* by GD-Chalcone, assessed using the Transwell assay; B: Quantification of HCC cells migration using the Transwell assay; C: Inhibition of HCC cells migration *in vitro* by GD-Chalcone, assessed using the scratch assay; D: Quantification of HCC cell migration using the scratch assay; E: Inhibition of HCC cell proliferation *in vitro* by GD-Chalcone, assessed using the clonogenic assay; F:

DOI: 10.20517/scierxiv202505.0135.v1

Quantification of HCC cell proliferation using the clonogenic assay. $^{ns}P > 0.05$, $^{*}P<0.05$, $^{**}P<0.01$, $^{***}P<0.001$, and $^{****}P<0.0001$.

DOI: 10.20517/scierxiv202505.0135.v1

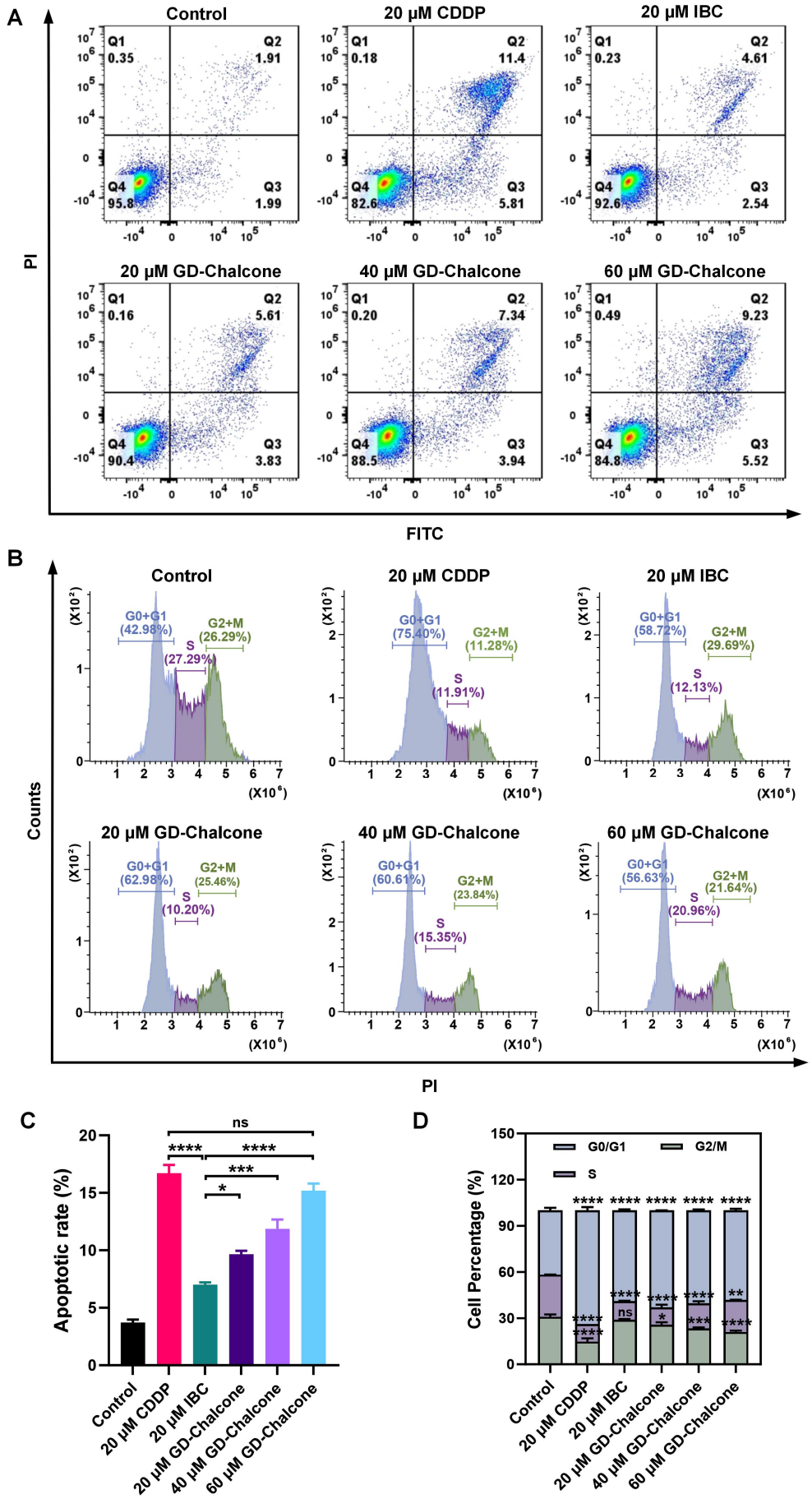

DOI: 10.20517/scierxiv202505.0135.v1

Figure 3. Effects of GD-Chalcone on HCC cell apoptosis and proliferation. A: GD-Chalcone-induced apoptosis in HCC cells *in vitro*, assessed using the cellular apoptosis assay with FCM; B: Impact of GD-Chalcone on HCC cell proliferation and cell cycle progression *in vitro*, evaluated using the cell cycle assay with FCM; C: Quantification of early and late apoptotic/necrotic cells using the FCM apoptosis assay; D: Distribution of cell cycle phases determined by the FCM cell cycle assay. $^{ns}P>0.05$, $^{*}P<0.05$, $^{**}P<0.01$, $^{***}P<0.001$, and $^{****}P<0.0001$.

In vivo therapeutic effects of GD-Chalcone

To evaluate the *in vivo* therapeutic effects of GD-Chalcone, we established hepatoma mice models using DEN induction. The mice treated with GD-Chalcone showed some recovery in their body weight compared to the model group (Figure 4A). Compared with the normal group, the liver surface of the model group appeared significantly rougher with white lesions (Figure 4B). HE staining results also showed evident pathological changes in the liver of the model group, including clustered cancer cells with pronounced atypia, a trabecular arrangement, rich sinusoidal stroma, and irregularly shaped structures. Abnormal mitotic figures and giant tumor cells were also observed. Compared with the model group, treatment with 40 mg/kg GD-Chalcone showed certain therapeutic effects, and pathological changes in the liver tissue were alleviated. An orderly arrangement of hepatocytes , nearly normal nuclear morphology, significantly reduced infiltration of inflammatory cells, and more intact liver lobule structure was observed. The effects were also marginally better than those of the 20 mg/kg Sor group (Figure 4C). These results suggested that GD-Chalcone may have protective effects on the liver and help reduce liver damage.

In addition, we evaluated the effects of different treatments on the expression of alpha-fetoprotein (AFP) in liver tissues of mice using immunohistochemical staining (Figure 4D). The results showed that compared with the normal group, the expression of AFP in the model group was significantly enhanced, which is consistent with abnormal

DOI: 10.20517/scierxiv202505.0135.v1

hepatocyte proliferation or tumor formation. The AFP expression in the sorafenib-treated group was reduced, indicating a certain therapeutic effect. However, the AFP expression in the GD-Chalcone-treated group was further decreased, particularly at the dose of 4 mg/kg, where the effect was superior to that of the 20 mg/kg sorafenib group. These results suggest that GD-Chalcone may be more effective in reducing AFP expression, thereby supporting its potential as a therapeutic agent.

Safety evaluation of GD-Chalcone *in vitro* and *in vivo*

The safety of GD-Chalcone was systematically evaluated *in vitro* and *in viv*o using cytotoxicity assays, hemolysis tests, and gut microbiota analysis. The results showed that GD-Chalcone exhibited relatively low toxicity to NRK-52E and fibroblast cells and weak hemolytic effects on RBCs. Hemolysis rates remained below 5% at both high and low concentrations (Figures 5A-C).

GD-Chalcone also partially restored gut microbiota homeostasis (Figures 5D-F). Compared with the model group, treatment with GD-Chalcone significantly increased the abundance of *Muribaculaceae*, a genus known for producing short-chain fatty acids (SCFAs) and maintaining gut health[16] (Figure 5G). The microbiota richness was also more effectively restored in the GD-Chalcone treatment group compared with the Sor group (Figure 6). These results provided crucial safety data supporting the clinical application of GD-Chalcone.

DOI: 10.20517/scierxiv202505.0135.v1

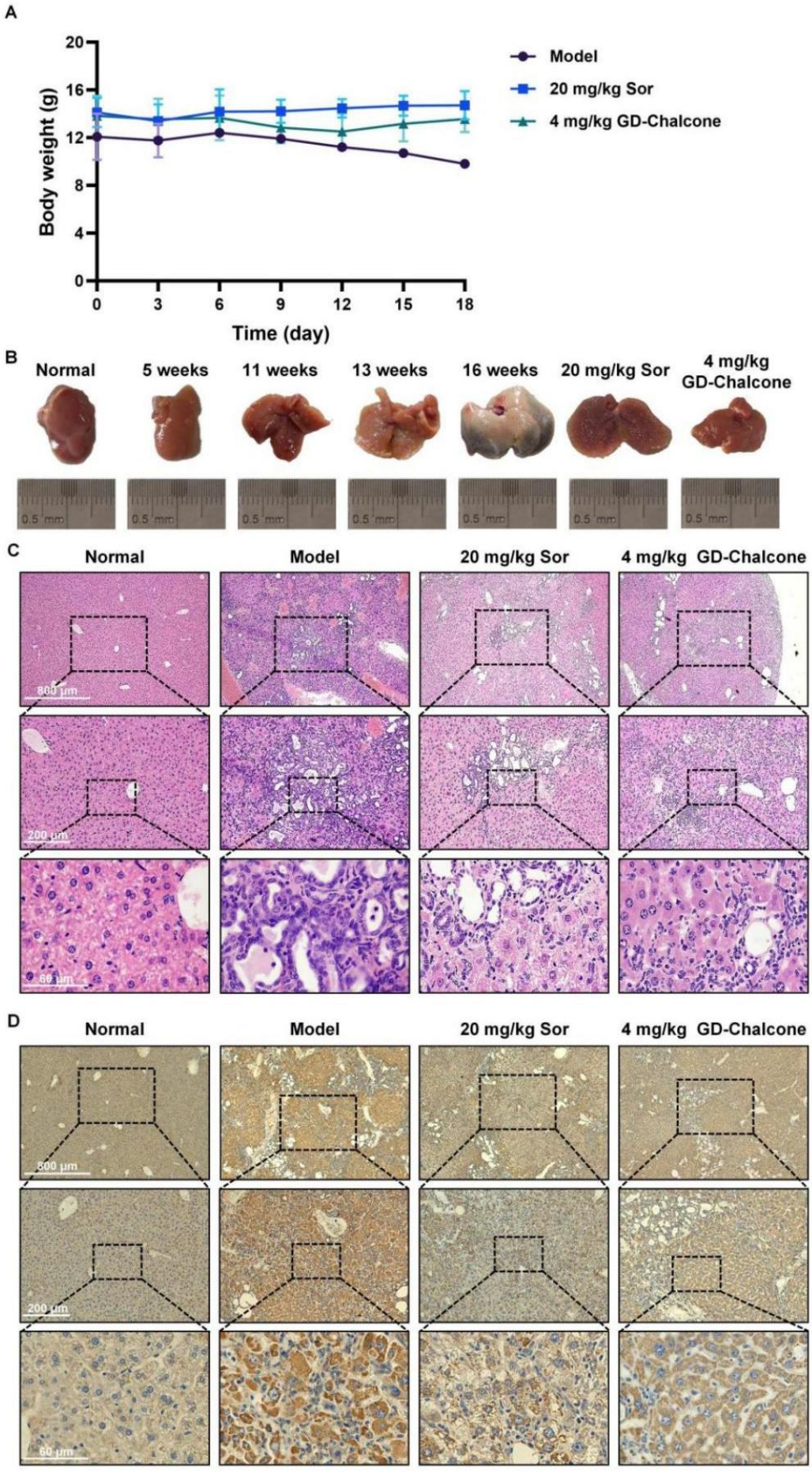

DOI: 10.20517/scierxiv202505.0135.v1

Figure 4. Therapeutic effects of GD-Chalcone on mice with hepatoma. A: Body weight measurements of mice with hepatoma in different treatment groups; B: Morphological changes in the livers of mice at different stages; C: Pathological sections of liver tissues from mice in different treatment groups (H&E staining); D: Immunohistochemical analysis of alpha-fetoprotein (AFP) expression in mouse liver tissue.

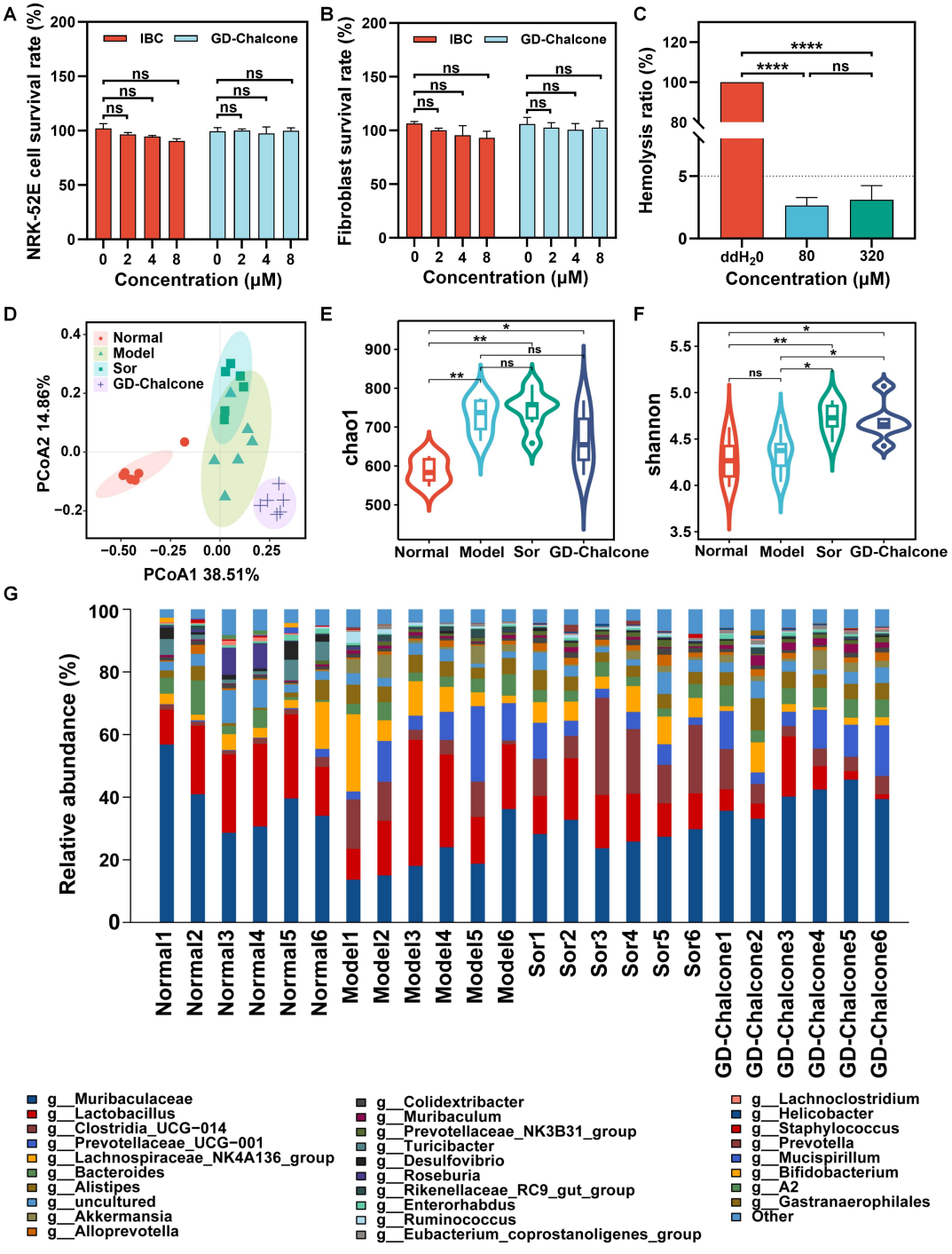

DOI: 10.20517/scierxiv202505.0135.v1

Figure 5. Evaluation of GD-Chalcone safety *in vitro* and diversity of flora *in vivo*. A: Safety evaluation of NRK-52E cells; B: Safety evaluation of fibroblasts; C: Hemolysis assay of GD-Chalcone; D: Principal Coordinates Analysis (PCoA); E: Chao1 diversity index analysis; F: Shannon diversity index analysis; G: Species composition analysis at the genus level. $^{ns}P>0.05$, $^{*}P<0.05$, $^{**}P<0.01$, $^{***}P<0.001$, and $^{****}P<0.0001$.

DOI: 10.20517/scierxiv202505.0135.v1

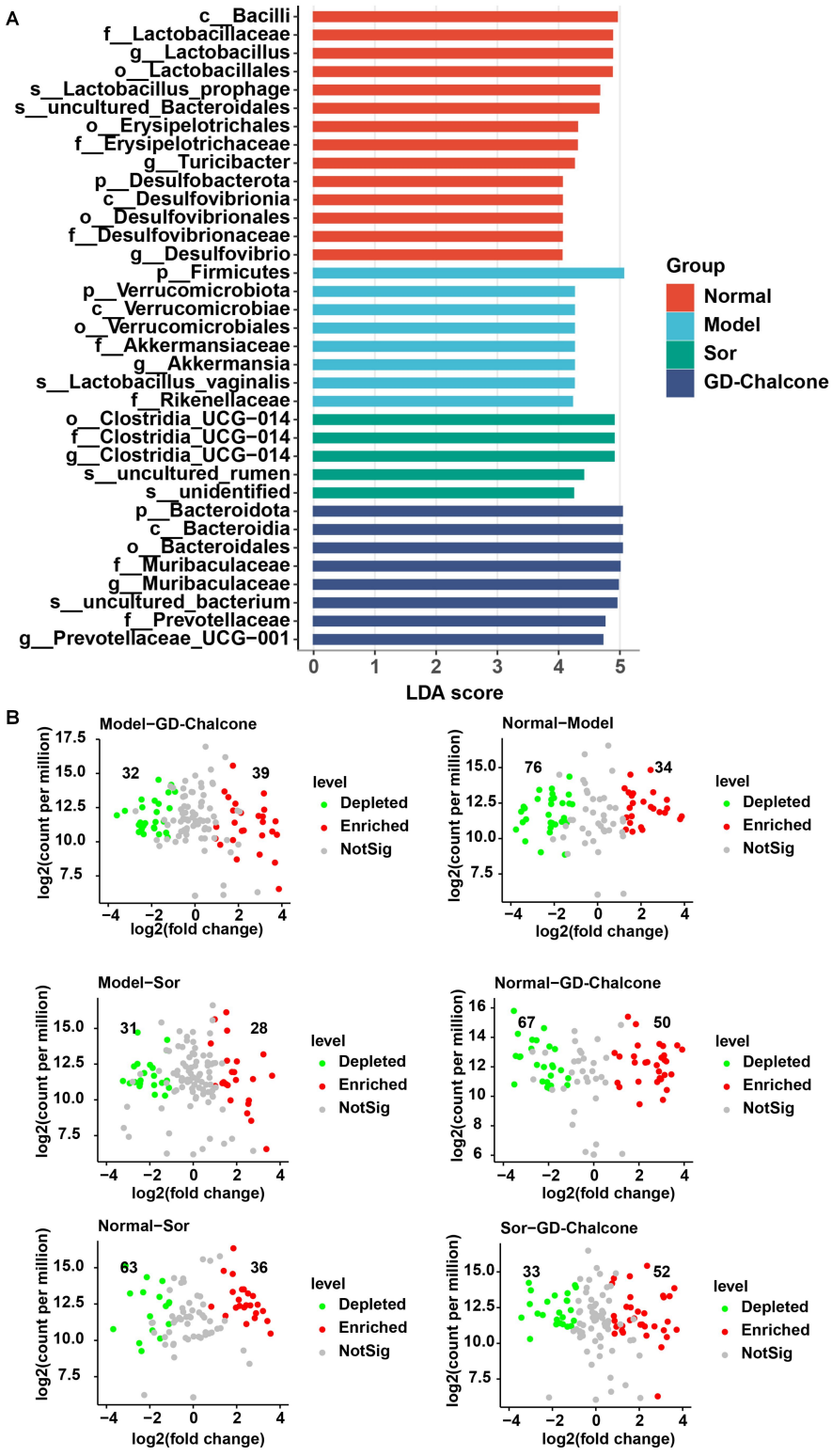

Figure 6. The effects of GD-Chalcone on the richness of intestinal microbiota. A: Linear discriminant analysis (LDA) effect size; B: EdgeR analysis.

Mechanism of action of GD-Chalcone

DOI: 10.20517/scierxiv202505.0135.v1

Targets for GD-Chalcone (n = 100) were identified in the SwissTargetPrediction database. In the GeneCards database, 9,910 known targets related to SMMC-7721 cells were identified, of which 89 targets were shared (Figure 7A). The GO enrichment analysis of these 89 shared targets suggested that GD-Chalcone may influence cellular phosphorylation regulation. GD-Chalcone may also induce apoptosis by inhibiting the negative feedback regulation of the apoptosis process in tumor cells. It was associated with the positive regulation of cell proliferation and migration (Figure 7B). The network diagram displayed 85 potential targets of GD-Chalcone in SMMC-7721 cells (Figure 7C). Molecular docking results also showed that the classic apoptotic proteins, Bcl-2-associated X (Bax) and B-cell lymphoma 2 (Bcl-2), exhibited a binding affinity with GD-Chalcone (Figures 7E and F).

The KEGG analysis suggested that GD-Chalcone may have been involved in regulating the calcium ion (Ca^{2+}) signaling pathway, mitogen-activated protein kinase (MAPK) signaling pathway, and phosphoinositide 3-kinase-protein kinase B (PI3K-Akt) signaling pathway, all of which may influence cell proliferation and apoptosis (Figure 7D). In summary, heat shock protein 90 alpha family class A member 1 (HSP90AA1) and epidermal growth factor receptor (EGFR), identified as strongly associated targets with GD-Chalcone, have both been confirmed as key targets for the treatment of liver cancer[17,18]. They are also related to cell proliferation and apoptosis[19,20]. Further research will be conducted focusing on these targets.

To validate the regulatory effect of GD-Chalcone on apoptosis-related genes, we conducted real-time PCR analysis of Bcl-2 and Bax expression (Figure 8). The results revealed that GD-Chalcone significantly downregulated the mRNA expression of the anti-apoptotic gene Bcl-2 while upregulating the pro-apoptotic gene Bax. These findings further confirm the role of GD-Chalcone in promoting apoptosis in SMMC-7721 cells, consistent with the molecular docking results and KEGG pathway analysis.

DOI: 10.20517/scierxiv202505.0135.v1 https://www.scierxiv.com/

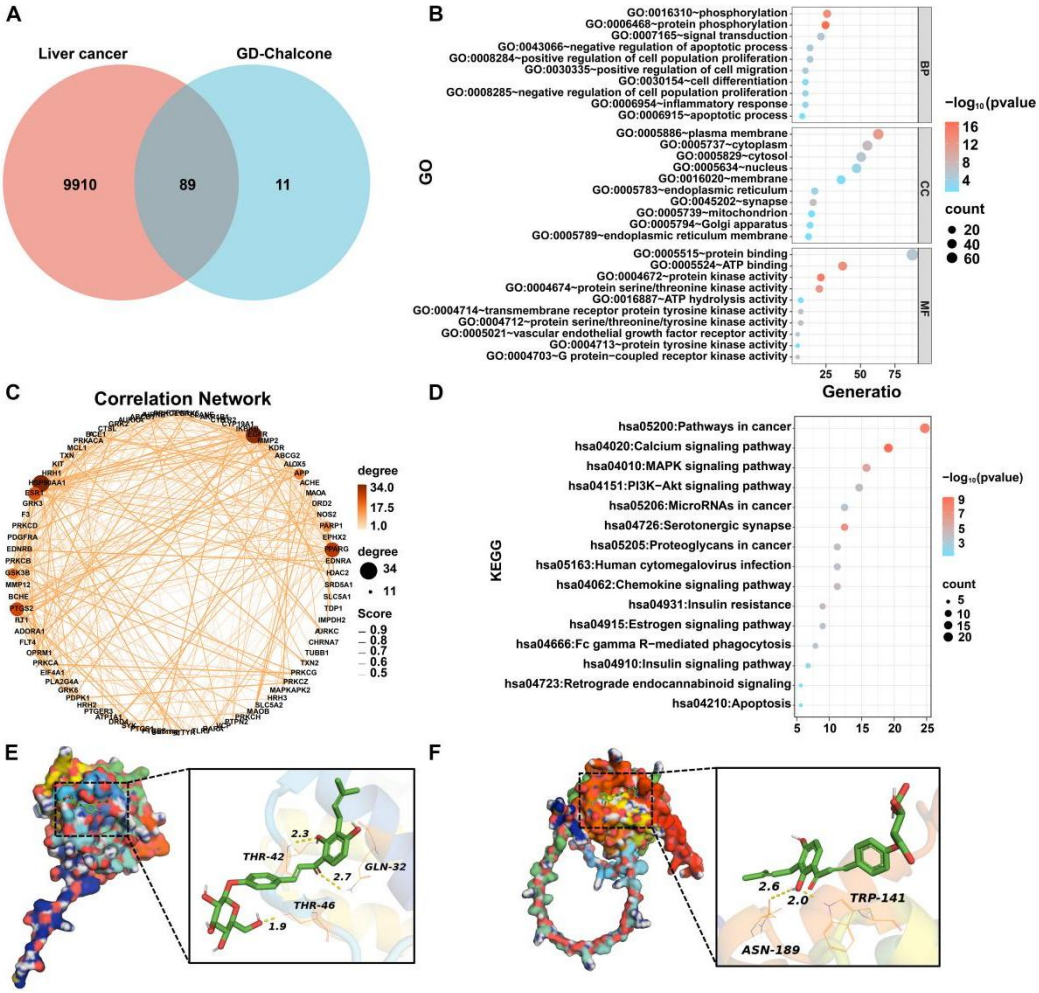

Figure 7. Mechanism of action of GD-Chalcone. A: Venn analysis; B: GO analysis; C: PPI analysis; D: KEGG analysis; E: Visualization of the docking results between Bax and GD-Chalcone; F: Visualization of the docking results between Bcl-2 and GD-Chalcone.

DOI: 10.20517/scierxiv202505.0135.v1

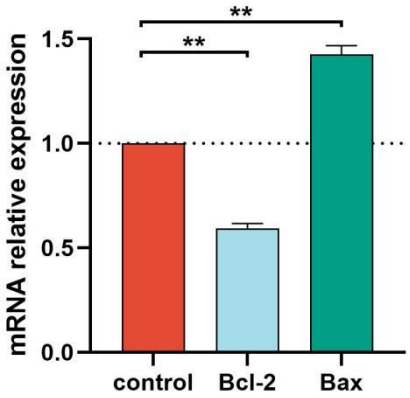

Figure 8. Real-time PCR assays validation.

DISCUSSION

In this study, we synthesized GD-Chalcone by introducing a brominated glucoside group to chalcone, enhancing its solubility and bioactivity. The molecular structure of GD-Chalcone was confirmed through LC-MS, NMR, carbon nuclear magnetic resonance (CNMR), and FTIR analyses. Compared to IBC, GD-Chalcone demonstrated significantly improved solubility, providing a solid foundation for subsequent biological investigations.

The CCK8 assay revealed that GD-Chalcone exhibited potent inhibitory activity against HCC cells (SMMC-7721, HuH-7, and HepG2.2.15), with a particularly pronounced effect on SMMC-7721 cells, where the IC_{50} value was reduced by 3-4 times compared to IBC. Interestingly, GD-Chalcone showed reduced activity against MGC803 gastric cancer cells, suggesting a degree of selectivity toward HCC. These findings warranted further investigation into its mechanism of action in HCC.

In vitro studies demonstrated that GD-Chalcone effectively suppressed proliferation, invasion, and migration of HCC cells. Flow cytometry analysis confirmed that GD-Chalcone induced apoptosis and arrested the cell cycle in the S phase. The S phase is crucial for DNA replication, and its disruption can lead to replication stress, ultimately triggering apoptosis. This mechanism aligns with common anticancer

strategies that target DNA replication vulnerabilities in rapidly dividing cancer cells[21,22]. To further elucidate this mechanism, key regulatory proteins involved in S phase progression, including origin recognition complexes (ORCs), cell division cycle 6 (CDC6), chromatin licensing and DNA replication factor 1 (CDT1), minichromosome maintenance complexes (MCMs), chromatin assembly factor 1 (CSC), GINS complex (GINS), DBF4-dependent kinase (DBF4-CDC7), and cyclin E-dependent kinase 2 (Cyclin E-CDK2)[23,24], will be examined in future studies.

In vivo experiments using the DEN-induced HCC model showed that GD-Chalcone significantly mitigated liver surface abnormalities, improved histopathological features, and restored gut microbiota composition. Its effects were comparable to those of sorafenib, further supporting its therapeutic potential. Moreover, GD-Chalcone contributed to body weight maintenance and exhibited no significant toxicity, as confirmed by cytotoxicity and hemolysis assays, suggesting a favorable safety profile.

A key biomarker for HCC, alpha-fetoprotein (AFP), is closely associated with tumor malignancy[25]. Our findings revealed that GD-Chalcone significantly reduced AFP expression, consistent with its inhibitory effects on HCC cell proliferation and migration[26]. Notably, GD-Chalcone exhibited superior efficacy in reducing AFP levels compared to sorafenib, underscoring its potential as a novel anti-HCC agent. However, while AFP reduction is an important indicator of therapeutic efficacy, it does not directly correlate with complete tumor regression. Future studies should explore the molecular mechanisms underlying GD-Chalcone-mediated AFP suppression and its broader implications for HCC treatment.

To investigate the molecular mechanisms of GD-Chalcone, bioinformatics analyses were performed. GO analysis indicated that GD-Chalcone was primarily associated with the the regulation of phosphorylation, apoptosis, and cell migration. KEGG pathway enrichment analysis revealed that GD-Chalcone exerts its effects on HCC cells through

multiple pathways, including calcium signaling, MAPK signaling, and PI3K/AKT signaling. These findings suggest a multi-targeted mechanism underlying its antitumor activity. Additionally, PPI analysis identified HSP90AA1 and EGFR as key targets, which are known to play pivotal roles in liver cancer progression and therapeutic resistance[27].

A major obstacle in HCC therapy is drug resistance, which significantly limits the efficacy of conventional chemotherapeutic agents. Various mechanisms contribute to resistance, including activation of survival pathways, upregulation of drug efflux transporters, epithelial-to-mesenchymal transition (EMT), and alterations in the tumor microenvironment[28]. The PI3K/AKT pathway is a well-established driver of chemoresistance, promoting cell survival and proliferation[29]. Our results demonstrated that GD-Chalcone effectively inhibits the PI3K/AKT pathway, suggesting its potential to counteract resistance mechanisms in HCC.

Moreover, apoptosis resistance in HCC is often linked to an imbalance between pro-apoptotic (Bax) and anti-apoptotic (Bcl-2) proteins. GD-Chalcone treatment resulted in Bax upregulation and Bcl-2 downregulation, thereby restoring apoptotic sensitivity. This mechanism is particularly relevant in overcoming resistance to apoptosis-inducing agents such as sorafenib. Future studies should explore whether GD-Chalcone also affects the expression of drug efflux pumps (e.g., ABC transporters), which play a critical role in reducing intracellular drug accumulation and promoting resistance.

Emerging research suggests that gut microbiota can influence drug resistance by modulating drug metabolism and immune responses[30]. Given that GD-Chalcone also affected gut microbiota composition, further investigations should focus on how these microbial changes contribute to its therapeutic efficacy. Understanding these interactions may enable the development of combination strategies that enhance the

effectiveness of GD-Chalcone in HCC therapy.

In conclusion, our study highlights the potent anti-HCC effects of GD-Chalcone, which not only inhibits tumor growth and metastasis but also exhibits promising potential for overcoming drug resistance. Further research is needed to validate its efficacy in drug-resistant HCC models and to explore potential combination therapies that could enhance its clinical utility.

DECLARATIONS

Acknowledgments

This research did not receive any specific grant from funding agencies in the public, commercial, or not-forprofit sectors. The authors thank the staff at Youjiang Medical University for Nationalities and Affiliated Hospital of Youjiang Medical University for Nationalities.

Authors' contributions

Investigation, data curation, formal analysis, writing- original draft preparation, visualization: Dai YY and Zhou WT.

Investigation, formal analysis, visualization: Luo JZ and Yang SX.

Methodology, writing - reviewing and editing: Liang SM.

Conceptualization, supervision, methodology, writing - reviewing and editing: Dou XB and Huang YQ.

Availability of data and materials

All data generated or analyzed in this study are included in this manuscript.

Financial support and sponsorship

This work was supported by the Guangxi Science and Technology Major projects (grant number AA23073012), the National Natural Science Foundation of China (grant numbers 32360035 and 32060018).

Conflicts of interest

All authors declared that there are no conflicts of interest.

Ethical approval and consent to participate

Ethical approval for this study was granted by the Youjiang Medical University for Nationalities Ethics Committee (Baise, China; approval No. 2024101801, approval on 28 September 2024).

Consent for publication

Not applicable.

Copyright

REFERENCES

1. Llovet JM, Kelley RK, Villanueva A, et al. Hepatocellular carcinoma. *Nat Rev Dis Primers* 2021;7:6.[DOI:10.1038/s41572-020-00240-3]
2. Sung H, Ferlay J, Siegel RL, et al. Global Cancer Statistics 2020: GLOBOCAN Estimates of Incidence and Mortality Worldwide for 36 Cancers in 185 Countries. *CA Cancer J Clin* 2021;71:209-49.[DOI:10.3322/caac.21660]
3. Choi JH, Thung SN. Advances in Histological and Molecular Classification of Hepatocellular Carcinoma. *Biomedicines* 2023;11:2582.[PMID:37761023 DOI:10.3390/biomedicines11092582 PMCID:PMC10526317]
4. Forner A, Reig M, Bruix J. Hepatocellular carcinoma. *Lancet* 2018;391:1301-14.[PMID:29307467 DOI:10.1016/s0140-6736(18)30010-2]

5. Llovet JM, Montal R, Sia D, Finn RS. Molecular therapies and precision medicine for hepatocellular carcinoma. *Nat Rev Clin Oncol* 2018;15:599-616.[PMID:30061739 DOI:10.1038/s41571-018-0073-4]
6. Jing F, Li X, Jiang H, Sun J, Guo Q. Combating drug resistance in hepatocellular carcinoma: No awareness today, no action tomorrow. *Biomed Pharmacother* 2023;167:115561.[DOI:10.1016/j.biopha.2023.115561]
7. Manning BD, Toker A. AKT/PKB Signaling: Navigating the Network. *Cell* 2017;169:381-405.[PMID:28431241 DOI:10.1016/j.cell.2017.04.001 PMCID:PMC5546324]
8. Long J, Wang A, Bai Y, et al. Development and validation of a TP53-associated immune prognostic model for hepatocellular carcinoma. *EBioMedicine* 2019;42:363-74.[PMID:30885723 DOI:10.1016/j.ebiom.2019.03.022 PMCID:PMC6491941]
9. Newman DJ, Cragg GM. Natural Products as Sources of New Drugs over the Nearly Four Decades from 01/1981 to 09/2019. *J Nat Prod* 2020;83:770-803.[PMID:32162523 DOI:10.1021/acs.jnatprod.9b01285]
10. Maphetu N, Unuofin JO, Masuku NP, Olisah C, Lebelo SL. Medicinal uses, pharmacological activities, phytochemistry, and the molecular mechanisms of Punica granatum L. (pomegranate) plant extracts: A review. *Biomed Pharmacother* 2022;153:113256.[PMID:36076615 DOI:10.1016/j.biopha.2022.113256]
11. Song X, Tan L, Wang M, et al. Myricetin: A review of the most recent research. *Biomed Pharmacother* 2021;134:111017.[DOI:10.1016/j.biopha.2020.111017]
12. Russo M, Spagnuolo C, Tedesco I, Russo GL. Phytochemicals in cancer prevention and therapy: truth or dare? *Toxins (Basel)* 2010;2:517-51.[PMID:22069598 DOI:10.3390/toxins2040517 PMCID:PMC3153217]
13. Guo L, Dong Z, Zhang X, et al. Morusinol extracted from Morus alba induces cell cycle arrest and apoptosis via inhibition of DNA damage response in melanoma by CHK1 degradation through the ubiquitin-proteasome pathway. *Phytomedicine* 2023;114:154765.[DOI:10.1016/j.phymed.2023.154765]

14. Chen L, Chen S, Sun P, Liu X, Zhan Z, Wang J. Psoralea corylifolia L.: a comprehensive review of its botany, traditional uses, phytochemistry, pharmacology, toxicology, quality control and pharmacokinetics. *Chin Med* 2023;18:4.[PMID:36627680 DOI:10.1186/s13020-022-00704-6 PMCID:PMC9830135]
15. Hao G, Zhai J, Jiang H, et al. Acetylshikonin induces apoptosis of human leukemia cell line K562 by inducing S phase cell cycle arrest, modulating ROS accumulation, depleting Bcr-Abl and blocking NF-κB signaling. *Biomed Pharmacother* 2020;122:109677.[DOI:10.1016/j.biopha.2019.109677]
16. Zhu Y, Chen B, Zhang X, et al. Exploration of the Muribaculaceae Family in the Gut Microbiota: Diversity, Metabolism, and Function. *Nutrients* 2024;16:2660.[PMID:39203797 DOI:10.3390/nu16162660 PMCID:PMC11356848]
17. Wang Z, Fan L, Xu H, et al. HSP90AA1 is an unfavorable prognostic factor for hepatocellular carcinoma and contributes to tumorigenesis and chemotherapy resistance. *Transl Oncol* 2024;50:102148.[PMID:39388959 DOI:10.1016/j.tranon.2024.102148 PMCID:PMC11736399]
18. Jin H, Shi Y, Lv Y, et al. EGFR activation limits the response of liver cancer to lenvatinib. *Nature* 2021;595:730-4.[DOI:10.1038/s41586-021-03741-7]
19. Liang Y, Zhang T, Ren L, et al. Cucurbitacin IIb induces apoptosis and cell cycle arrest through regulating EGFR/MAPK pathway. *Environ Toxicol Pharmacol* 2021;81:103542.[DOI:10.1016/j.etap.2020.103542]
20. Zhang MY, Ma LJ, Jiang L, et al. Paeoniflorin protects against cisplatin-induced acute kidney injury through targeting Hsp90AA1-Akt protein-protein interaction. *J Ethnopharmacol* 2023;310:116422.[DOI:10.1016/j.jep.2023.116422]
21. Gemble S, Wardenaar R, Keuper K, et al. Genetic instability from a single S phase after whole-genome duplication. *Nature* 2022;604:146-51.[PMID:35355016 DOI:10.1038/s41586-022-04578-4 PMCID:PMC8986533]

22. Petropoulos M, Karamichali A, Rossetti GG, et al. Transcription-replication conflicts underlie sensitivity to PARP inhibitors. *Nature* 2024;628:433-41.[PMID:38509368 DOI:10.1038/s41586-024-07217-2 PMCID:PMC11006605]
23. Armstrong C, Passanisi VJ, Ashraf HM, Spencer SL. Cyclin E/CDK2 and feedback from soluble histone protein regulate the S phase burst of histone biosynthesis. *Cell Rep* 2023;42:112768.[PMID:37428633 DOI:10.1016/j.celrep.2023.112768 PMCID:PMC10440735]
24. Fei L, Xu H. Role of MCM2-7 protein phosphorylation in human cancer cells. *Cell Biosci* 2018;8:43.[PMID:30062004 DOI:10.1186/s13578-018-0242-2 PMCID:PMC6056998]
25. Baskiran DY, Sarigoz T, Baskiran A, Yilmaz S. The Significance of Serum Tumor Markers CEA, Ca 19-9, Ca 125, Ca 15-3, and AFP in Patients Scheduled for Orthotopic Liver Transplantation: Do Elevated Levels Really Mean Malignancy? *J Gastrointest Cancer* 2023;54:442-6.[PMID:35312953 DOI:10.1007/s12029-021-00798-5]
26. Mao X, Wang J, Luo F. α-Fetoprotein contributes to the malignant biological properties of AFP-producing gastric cancer. *Open Life Sci* 2023;18:20220476.[PMID:37588998 DOI:10.1515/biol-2022-0476 PMCID:PMC10426758]
27. Liu L, Zheng Z, Huang Y, et al. HSP90 N-terminal inhibition promotes mitochondria-derived vesicles related metastasis by reducing TFEB transcription via decreased HSP90AA1-HCFC1 interaction in liver cancer. *Autophagy*. 2025;21:639-663. [PMID: 39461872 DOI: 10.1080/15548627.2024.2421703 PMCID: PMC11849932]
28. Wei CY, Zhu MX, Zhang PF, et al. Corrigendum to: "PKCα/ZFP64/CSF1 axis resets the tumor microenvironment and fuels anti-PD1 resistance in hepatocellular carcinoma" [J Hepatol 77 (2022) 163-176]. *J Hepatol* 2023;78:881-2.[DOI:10.1016/j.jhep.2022.11.004]

29. Sun Y, Zhang H, Meng J, et al. S-palmitoylation of PCSK9 induces sorafenib resistance in liver cancer by activating the PI3K/AKT pathway. *Cell Rep* 2022;40:111194.[DOI:10.1016/j.celrep.2022.111194]

30. Yao J, Ning B, Ding J. The gut microbiota: an emerging modulator of drug resistance in hepatocellular carcinoma. *Gut Microbes* 2025;17:2473504.[PMID:40042184 DOI:10.1080/19490976.2025.2473504 PMCID:PMC11901387]